catalysts

MDPI

Article

Optimization of the Washcoat Slurry for Hydrotalcite-Based LNT Catalyst

Yue Zhu [1], Gang Lv [1,*], Chonglin Song [1], Bo Li [1], Yantao Zhu [1], Ye Liu [1], Wei Zhang [1] and Yuanhong Wang [2]

[1] State Key Laboratory of Engines, Tianjin University, Tianjin 300072, China
[2] Department of Information Engineering, Chaoyang Teachers College, Chaoyang 122000, China
* Correspondence: lvg@tju.edu.cn; Tel.: +86-22-27406842-8021

Received: 14 July 2019; Accepted: 16 August 2019; Published: 20 August 2019

Abstract: This work aimed to optimize the washcoat slurry for hydrotalcite-based lean NOx trap (LNT) catalyst. The effects of the slurry properties including pH, solid content, binder and additive on the hydrotalcite-based slurry viscosity were investigated. The particle size distribution of the optimal hydrotalcite-based slurry was measured. A cordierite material was used to coat the optimal slurry, and the washcoat was characterized by X-ray diffraction, scanning electron microscopy and N_2 adsorption. The optimal slurry containing Pt and Ba was coated on the cordierite for the preparation of hydrotalcite-based LNT catalyst, and the performances of this catalyst were evaluated by NOx storage test, temperature programmed desorption and NOx reduction. For comparison, the performance of the commercial LNT catalyst with Pt/BaO/Al_2O_3 was analyzed. After coating, the hydrotalcite-based washcoat was closely contacted with the support, being the main phase MgO and presenting a specific surface area of 86.3 m^2/g. The hydrotalcite-based LNT catalyst had better NOx storage and desorption ability, selectivity to N_2 and LNT efficiency than the Pt/BaO/Al_2O_3 catalyst.

Keywords: slurry properties; viscosity; modified hydrotalcite; LNT; catalyst activity

1. Introduction

Given the increasing concern on energy conservation and pollution emissions, the utilization of lean NOx trap (LNT) is perceived as a promising way to effectively remove NOx emissions from diesel and lean burn gasoline engines. The LNT system, which was initially proposed by Toyota in 1996, mainly works under cyclic engine conditions by shifting long lean stages with short rich phases [1–3]. During lean conditions, NO is oxidized into NO_2 over precious metal and adsorbed on the LNT catalyst mainly in a form of nitrates. Periodically, the exhaust is switched into rich conditions for few seconds in order to reduce the stored NOx into N_2 [4]. Generally, the LNT catalyst consists of precious metals (such as Pt or/and Rh), adsorbents (such as oxides of Ba, K and Ca) and supports with high specific surface area like Al_2O_3 [5]. For the commercial LNT catalyst (Pt/BaO/Al_2O_3), it is hard to expand the catalytic and adsorption performances due to the low reactive activity and poor NOx uptake ability under low temperature conditions ($T \leq 250$ °C) [6]. Besides, the Pt/BaO/Al_2O_3 LNT catalyst presents deactivation for SO_2 resistance performance under high temperature conditions [7]. Consequently, it is necessary to develop the LNT catalysts with better catalytic performance under low, moderate and high temperature conditions.

Hydrotalcite-like compounds (HTLCs), which are mainly made up of layered double hydroxides, are now used worldwide in practical applications such as adsorbents, ion exchangers, base catalysts and precursors of mixed oxides for various catalytic applications [8,9]. The chemical formula of hydrotalcite-like compounds is $[M_{1-x}^{II}M_x^{III}(OH)_2]^{x+}[A^{n-}]_{x/n}\cdot mH_2O$. The numerical value of the coefficient x depends on the molar ratio of $M^{III}/(M^{II} + M^{III})$ [10]. The HTLCs can form a layered double

oxide (denoted as LDO) with high alkalinity and surface area after calcination. The LDO is an excellent support of LNT catalysts in the low-temperature NOx reactivity, SO_2-resistance performance and simultaneous reduction for both NOx and PM [11].

Studies have performed on improving the performance of hydrotalcite-based LNT catalysts through replacement of M^{II} by Cu^{2+}, Co^{2+}, Mn^{2+}, Ni^{2+} [12–15], substitution of M^{III} with other cations such as Fe or Cr [16,17] and even alteration of both M^{II} and M^{III} simultaneously [18–20]. These studies paid more attention on the impact of material modification on the catalytic performance of the LNT system, but rarely focused on the slurry properties. In general, an inadequate slurry could cause the separation of washcoat from the support surface or damage the cohesion strength within the washcoat and consequently worsen the catalytic performance [21,22]. The slurry properties, such as pH, solid content, binder and additive, are closely related to the washcoat distribution on the cordierite surface. Blachou et al. [23] prepared the washcoat slurry with γ-Al_2O_3 powder (3.3 μm) and revealed the relation between pH and slurry viscosity. They recommended a pH of 3.7 and a solid content of 42 wt% to obtain a wash coat loading between 18 to 22 wt% with a two-time impregnation. Shimrock et al. [24] coated the alumina slurry on the inner surface of honeycomb substrates, and found that a solid content between 35 to 52 wt% favored the achievement of a much more uniform washcoat loading. Gao et al. [25] synthesized the alumina slurry with SB powder (a pseudoboehmite-type aluminum hydroxide) and HNO_3 to investigate the effects of additives on slurry properties. They suggested that a more steady and homogeneous slurry could be achieved using an additive content of 2 wt%.

Up to present date, there are several studies about the effects of the alumina slurry properties on coating, but almost no data are available about the hydrotalcite-based slurry. The purpose of this paper is to shed light on the effects of the hydrotalcite-based slurry properties on slurry viscosity, coating and catalytic performance of the LNT system. The property parameters of hydrotalcite-based slurry include pH, solid content, binder and additive. In our previous work, an innovative hydrotalcite-based LNT catalyst, Pt/BaO/$Cu_{0.6}Mg_{2.4}Fe_{0.5}Al_{0.5}O$, was found to possess prominent performance in NOx removal [26]. Therefore, the $Cu_{0.6}Mg_{2.4}Fe_{0.5}Al_{0.5}O$ hydrotalcite oxides (denoted as CuMgFeAlO) were used for slurry preparation. A cordierite material was used to coat an optimal slurry, and the washcoat was characterized by X-ray diffraction (XRD), scanning electron microscopy (SEM) and N_2 adsorption. In addition, the optimal hydrotalcite-based slurry containing Pt and Ba was coated on the cordierite material for the preparation of the hydrotalcite-based LNT catalyst, and the activity of this catalyst was evaluated. At the same time, the performance of the commercial LNT catalyst with Pt/BaO/Al_2O_3 was analyzed.

2. Results and Discussion

2.1. Factors Affecting Slurry Viscosity

Viscosity is regarded as a major parameter governing the flow performance of slurry. A slurry with high viscosity has poor fluidity and can cause the heterogeneity of washcoat loaded on the surface of cordierite. However, a slurry with low viscosity also results in low washcoat loading. Because the slurry viscosity is generally determined by pH, solid content, binder and additive, the relationship between these factors and viscosity are investigated in the following sections.

2.1.1. pH

Figure 1 shows the effect of pH on the hydrotalcite-based slurry viscosity. The curve shown in Figure 1 was plotted by approaching the data points in a B-spline method embedded in the Origin software (9.0, OriginLab, Northampton, MA, USA, 2012). Such a method was also performed in Figures 2–5 and Figure 10. Here, glacial acetic acid is used for pH adjustment, and no binder and additive are included in the slurry. Agrafiotis et al. [27] studied the effect of solid content on the alumina-based slurry, and found that a solid content of 10 wt% was suitable for homogeneous coating. Beyond this value, the viscosity of the alumina-based slurry dramatically increased, and the

homogeneity of washcoat deteriorated. According to the findings of Agrafiotis et al., a solid content of 10 wt% is used in the hydrotalcite-based slurry in this study. As shown in Figure 1, the slurry exhibits alkalinity with a pH close to 12 in the absence of glacial acetic acid. The slurry viscosity changes obviously by the presence of glacial acetic acid, with a maximum of 75 mPa·s at pH = 9. This behavior may be related to the reaction between CO_3^{2-} and H^+, which generates CO_2 and causes volume expansion and temperature increment [28].

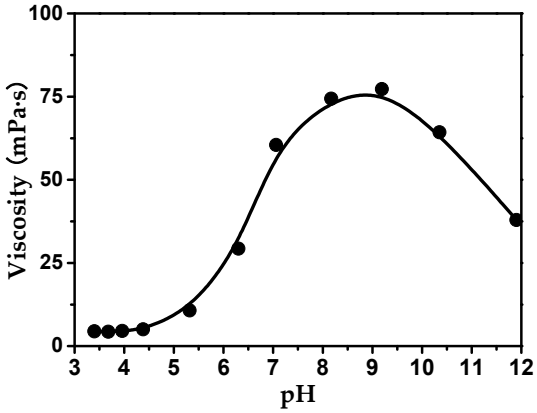

Figure 1. Slurry viscosity as a function of pH (solid content = 10 wt%, no binder, no additive).

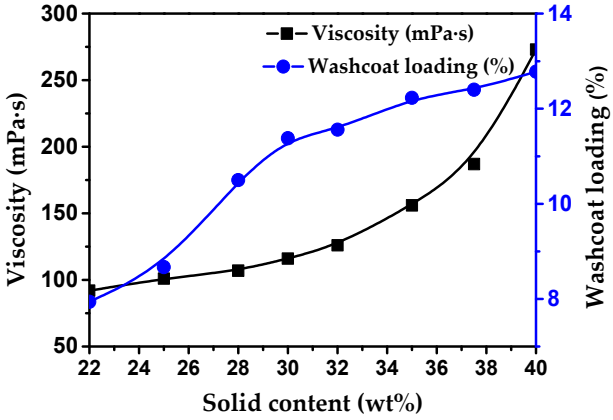

Figure 2. Slurry viscosity and washcoat loading as functions of solid content (pH = 4, no binder, no additive).

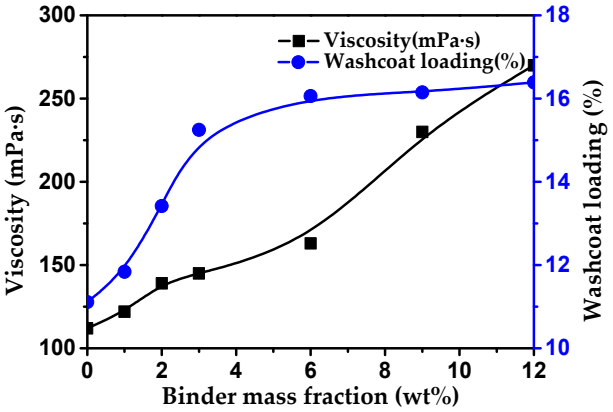

Figure 3. Slurry viscosity and washcoat loading as functions of binder mass fraction (pH = 4, solid content = 30 wt%, no additive).

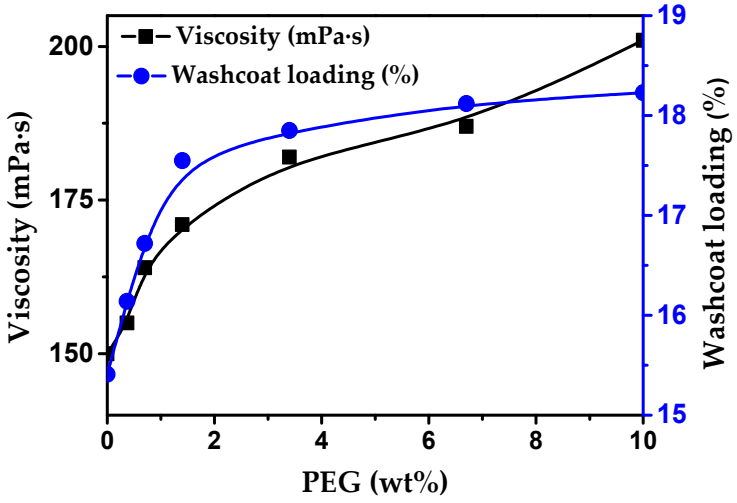

Figure 4. Slurry viscosity and washcoat loading as functions of PEG1000 content (pH = 4, solid content = 30 wt%, binder = 4 wt%).

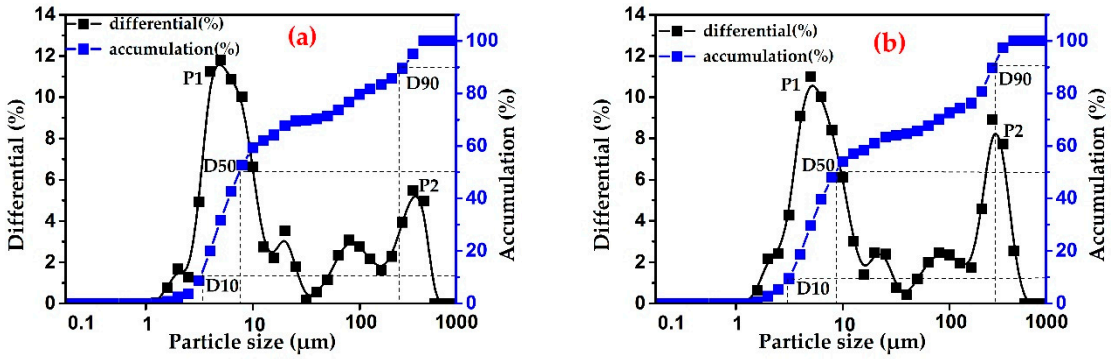

Figure 5. Particle size distribution in different slurries (**a**) sample (a); (**b**) sample (b).

In the present work, the slurry is composed of the hydrotalcite-based metal oxides, binder and additive. It should be noted that all these ingredients can influence the pH. To avoid the influence of pH on slurry viscosity, it is advisable to pick a range of pH in which the viscosity is nearly unchangeable. In Figure 1, the slurry viscosity almost holds constant at pH < 4.5, suggesting that the slurry viscosity is not sensitive to pH. In addition, Pereda-Ayo et al. [29,30] revealed that at pH = 3.5–4, the alumina-based slurry presented an optimal state of uniformity and stabilization, and a high washcoat loading could be achieved. Nijhuis et al. [22] reported that a pH of 3–4 could improve the slurry stabilization, while higher or lower pH increased the viscosity, resulting in unfavorable coating. Therefore, it is suitable to choose pH = 4 in the slurry preparation process.

2.1.2. Solid Content

Figure 2 shows the slurry viscosity and washcoat loading as functions of the solid content (i.e., the hydrotalcite-based oxides, denoted as CuMgFeAlO). Obviously, the slurry viscosity increases with increasing solid content, and a significant increase in viscosity is obtained in the case of the high solid content. In addition, the washcoat loading increases with an increase in solid content, especially at solid content < 30 wt% where the washcoat loading sharply increases with the increased solid content. In fact, a high solid content can cause some detrimental consequences such as uneven washcoat thickness, separation of washcoat from cordierite and even blockage of partial support channels [31]. Therefore, a solid content of 30 wt% is advisable in the slurry preparation process.

2.1.3. Binder Mass Fraction

Figure 3 shows the slurry viscosity and washcoat loading as functions of binder mass fraction. Here, alumina sol is used as the binder. As seen in Figure 3, the slurry viscosity shows a distinct increase with binder mass fraction. Moreover, the washcoat loading increases with an increase in binder mass fraction. It should be noted that at the binder content > 4 wt%, no significant increase in washcoat loading is obtained. Adamowska et al. [32] reported that the slurry with high binder mass fraction was extremely difficult to disperse homogeneously on the surface of support, and at the same time could result in some terrible consequences such as channel block and falling off of washcoat. Therefore, a binder mass fraction of 4 wt% is used for the slurry preparation.

2.1.4. Additive Content

In the preparation of washcoat slurry, additive is utilized to improve the performance of slurry and/or the adhesion and stability of washcoat layers. In this work, polyethylene glycol (PEG1000) was selected as additive. Figure 4 shows the slurry viscosity and washcoat loading as functions of the PEG1000 content. Obviously, the slurry viscosity increases with the PEG1000 content. This behavior can be attributed to the hydrogen bond created between the polyoxyethylene in the PEG1000 and the hydroxyl groups on the surface of colloidal particles, which strengthens the attraction among the colloidal particles [33]. Besides, it can be seen from Figure 4 that the addition of PEG1000 results in an increase in the washcoat loading, but it is very slight when PEG1000 content > 2 wt%. Actually, the large PEG1000 content will deteriorate the slurry fluidity, and cause a difficulty in coating. Gao et al. [25] investigated the effects of additives on the properties of the alumina slurry, and found that a steady and homogeneous slurry could be achieved at additive content = 2 wt%. Therefore, a PEG1000 content of 2 wt% is utilized for the slurry synthesis.

2.2. Particle Size Distribution

Previous reports [28–31] confirmed that the consistency of slurry could be strengthened by narrowing the distribution of particle size, and therefore the adhesion firmness between the support and the washcoat layer would be improved. In this section, the particle size distribution of the optimal hydrotalcite-based slurry was investigated. For comparison, the hydrotalcite powder was dissolved in deionized water to prepare a single-component slurry. The descriptions of both slurries are listed in Table 1.

Table 1. The description of different hydrotalcite-based slurries.

Sample	Main Composition	Other Composition(s)
a	CuMgFeAlO	Deionized water
b [1]	CuMgFeAlO	Deionized water, glacial acetic acid, alumina sol and PEG1000

[1] The detailed parameters are given as follows: pH = 4, solid content = 30 wt%, binder = 4 wt% and PEG1000 = 2 wt%.

In Figure 5, the particle size distribution for sample (a) and (b) exhibit multiple peaks, indicating a wide particle size distribution. After the addition of other materials including glacial acetic acid, alumina sol and PEG1000, the major peak P1 is slightly lower, but the secondary peak P2 becomes higher. This behavior is probably due to the non-homogeneous blend and agglomeration of the components in the slurry [34].

For comparison, D10, D50 and D90 are employed to characterize the features of particle size distribution. Herein, the value of Dxx represents a particle size for which xx% of the particles are finer [35]. The blue line in Figure 5 represents the accumulative distributions of the particle sizes. It is calculated by a cumulative sum of the number percentages corresponding to the particles smaller than a certain particle size. D10, D50 and D90 of both slurries are given in Table 2. The particle size in D10, D50 and D90 for sample (b) are almost the same as compared to sample (a). This result indicates that

there is no significant impact on the particle size distribution after the addition of glacial acetic acid, alumina sol and PEG1000.

Table 2. Parameters of particle size distribution in the slurries.

Sample	D10 (μm)	D50 (μm)	D90 (μm)
a	2.96	6.84	303.54
b	2.82	7.08	307.13

2.3. Characterization of Catalyst Washcoat

The optimized hydrotalcite-based slurry was coated on the surface of cordierite material, and, as reference, a raw cordierite without washcoat was also prepared. After being dried and calcined, the samples were cut into small blocks or milled into powder for SEM, XRD and BET tests.

2.3.1. SEM

The typical SEM images of the hydrotalcite-covered and alumna-covered cordierite support are shown in Figure 6. Both washcoats uniformly disperse on the surface of cordierite support, as seen in Figure 6a1,b1. The longitudinal sections of both washcoat-supports in Figure 6a2,b2 show a rough cordierite skeleton accompanied by pores with different diameters. In addition, the washcoats embedded in the support apertures strengthen the adhesion between the washcoat and cordierite material. In Figure 6a3, it can be seen that no obvious crack exists on the surface of the hydrotalcite-based washcoat, which suggests that the stress caused by the different thermal expansion coefficients between cordierite and washcoat has no significant impact on washcoat stability [30]. In Figure 6b3, an obvious crack is observed on the surface of the alumina-covered support. Figure 6a4 demonstrates that the lamellar structure for the hydrotalcite-like materials [36] is still observed in the washcoat after calcination.

2.3.2. XRD Analysis

Figure 7 shows the XRD pattern of the hydrotalcite-based washcoat. The main phase in Figure 7 corresponds to MgO (JCPDS 45-0946). The appearance of MgO phase is due to the high content of Mg in the CuMgFeAlO material [37]. There are no other peaks to be found, suggesting that the Cu, Al and Fe uniformly disperse in the CuMgFeAlO material and exist mainly in a form of amorphism. According to the findings of Jabłońska et al. [37], the XRD pattern of the hydrotalcite-derived composite metal oxide only demonstrates the phase of MgO, which is related to the high content of Mg. The observation of the MgO phase in Figure 7 confirms the existence of CuMgFeAlO in the washcoat after calcination.

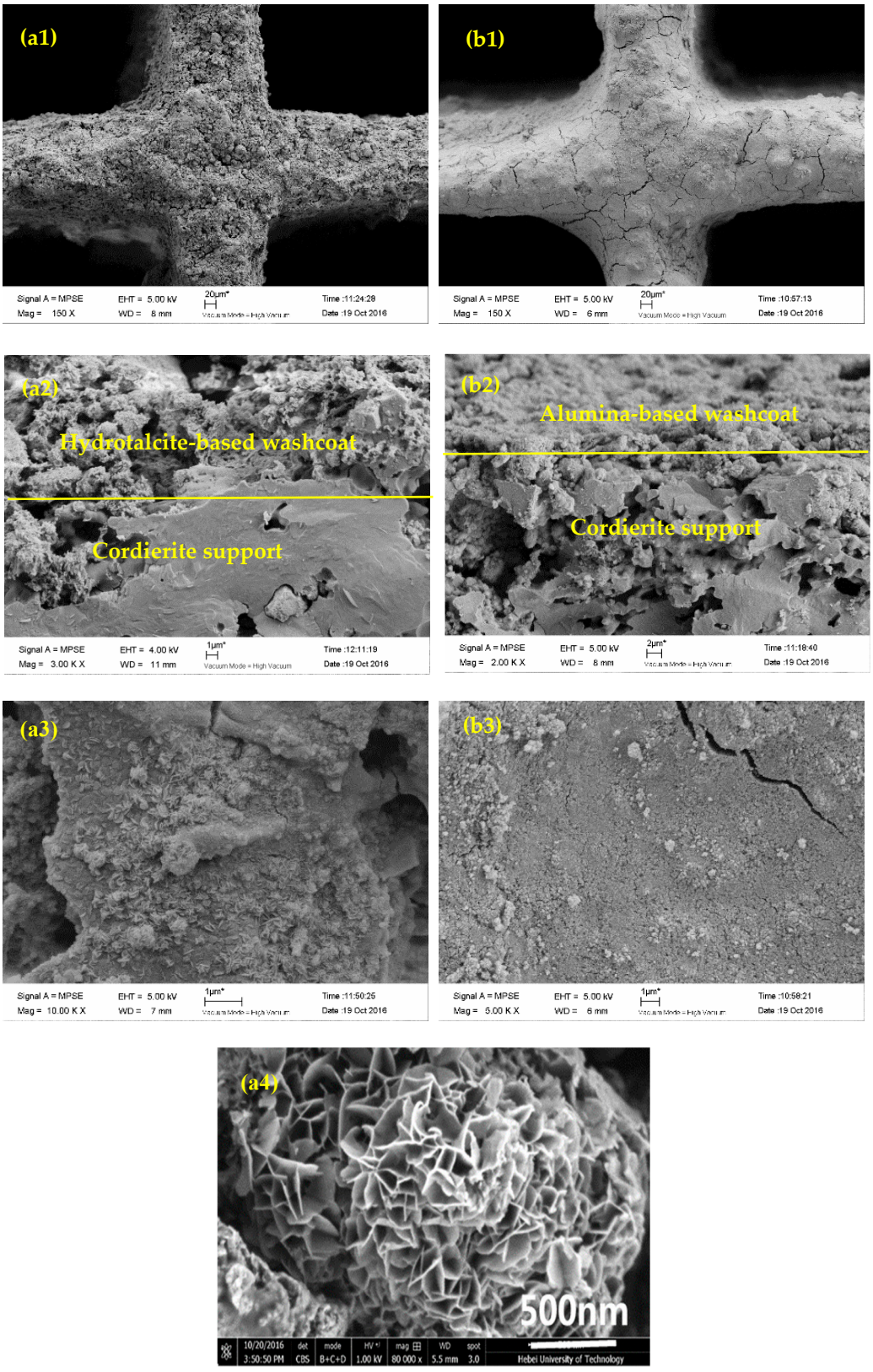

Figure 6. SEM images for the hydrotalcite-covered and alumina-covered cordierite supports. (**a1–a4**) Hydrotalcite-covered support; (**b1–b3**) alumina-covered support.

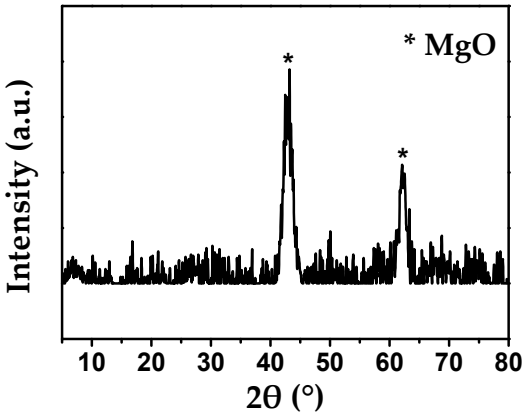

Figure 7. XRD pattern of the hydrotalcite-based washcoat.

2.3.3. BET Measurement

Table 3 shows the BET surface area for the cordierite supports. It can be seen that the fresh support exhibits a BET surface area of 0.93 m^2/g, while the BET surface area increases obviously after covering with the hydrotalcite-based washcoat, reaching a value of 86.3 m^2/g. This behavior is partially related to the addition of PEG1000, promoting the formation of a porous structure in the calcination process [34]. The BET surface area for the commercial alumina-based washcoat presents a value of 123.6 m^2/g, much higher than for the hydrotalcite-based washcoat.

Table 3. Specific surface area of cordierite ceramic honeycomb with washcoat.

Sample	Main Composition	BET (m^2/g)
a	Fresh cordierite support	0.93
b	Hydrotalcite-based washcoat, cordierite support	86.3
c	Alumina-based washcoat, cordierite support	123.6

2.4. Performance of the Monolithic Catalyst

In this work, the optimal hydrotalcite-based slurry containing Pt and Ba was coated on the surface of cordierite material for the preparation of the hydrotalcite-based LNT catalyst (Pt/BaO/CuMgFeAlO). In addition, the commercial LNT catalyst with Pt/BaO/Al_2O_3 was prepared for comparison. Multi-impregnation was used to achieve a washcoat loading of 25%. Both catalysts contained the identical contents of Pt (1 wt%) and BaO (20 wt%).

2.4.1. SEM

Figure 8 shows the representative SEM images of Pt/Ba/Al_2O_3 and Pt/BaO/CuMgFeAlO catalysts. Both the alumina-based and the hydrotalcite-based washcoats homogeneously disperse on the surface of cordierite, as found in Figure 8a1,b1. Figure 8a2 shows that a dense structure for the alumina-based washcoat is observed. For the Pt/BaO/CuMgFeAlO catalyst, the observation of original lamellar texture in Figure 8b2 suggests no significant changes of washcoat structure after calcination.

2.4.2. NOx Storage Capacity

The NOx concentrations at reactor outlet for the catalysts are shown in Figure 9. As expected, the NOx concentrations for both catalysts increase with the time as the catalysts gradually approach the adsorption saturation state. The outlet NOx concentrations for the Pt/BaO/CuMgFeAlO catalyst are consistently lower than for the Pt/BaO/Al_2O_3 catalyst in the range of studied temperatures. This result indicates that the Pt/BaO/CuMgFeAlO catalyst still maintains excellent performance in NOx storage after coating on the cordierite material.

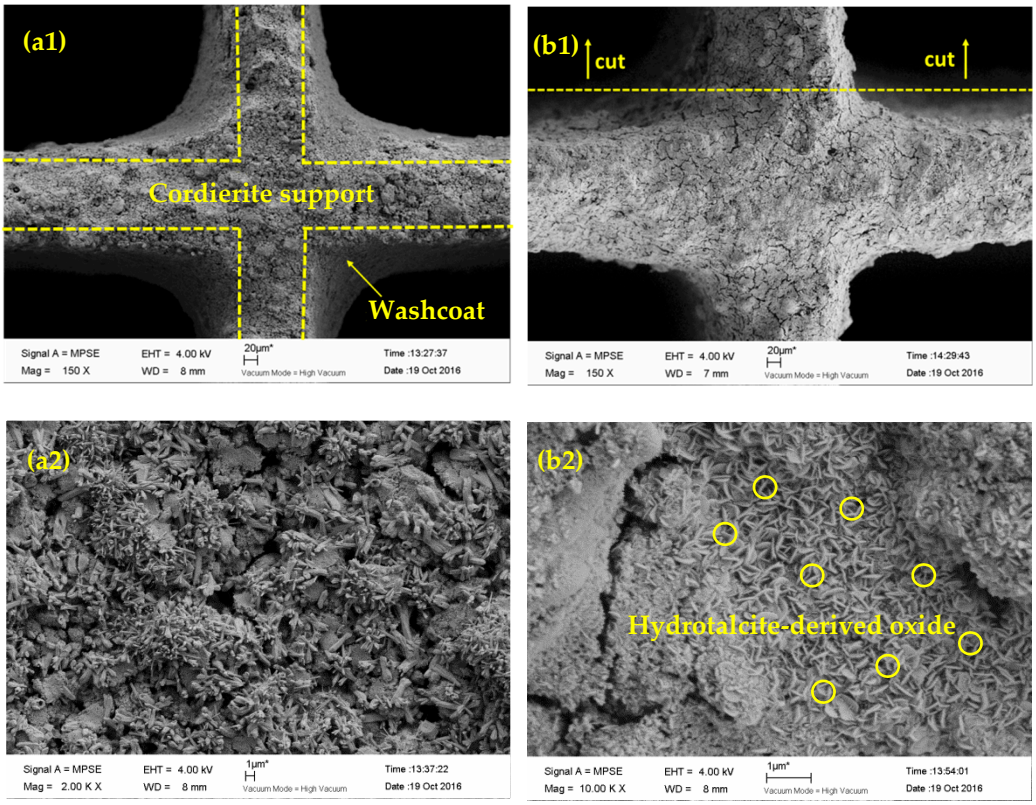

Figure 8. SEM images for both lean NOx trap (LNT) catalysts. (**a1**,**a2**) Pt/BaO/Al_2O_3; (**b1**,**b2**) Pt/BaO/CuMgFeAlO.

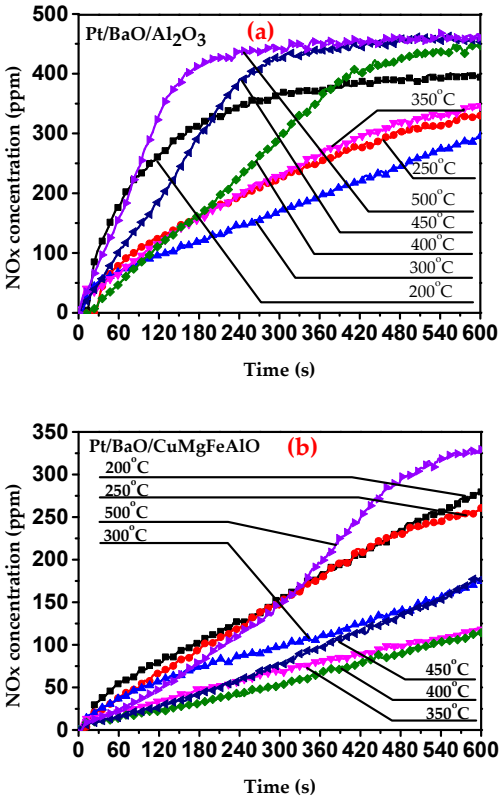

Figure 9. Outlet NOx concentration profiles for both LNT catalysts under different temperatures. (**a**) Pt/BaO/Al_2O_3; (**b**) Pt/BaO/CuMgFeAlO.

It was reported that the hydrotalcite-based catalyst had abundant adsorption sites on the transition metal oxides [38,39] and there was a synergistic effect between metal oxides and adsorption component [40], which improved the NOx storage ability of the catalyst. Similar results are obtained in this work. Figure 10 shows the NOx storage efficiency for both catalysts after adsorption of 2 and 10 min. For the Pt/BaO/CuMgFeAlO catalyst, a better NOx storage efficiency is observed in the range of test temperatures as compared to the Pt/BaO/Al_2O_3 catalyst. This result demonstrates that the optimization of slurry has no significant impact on the performance in NOx storage efficiency for the Pt/BaO/CuMgFeAlO catalyst.

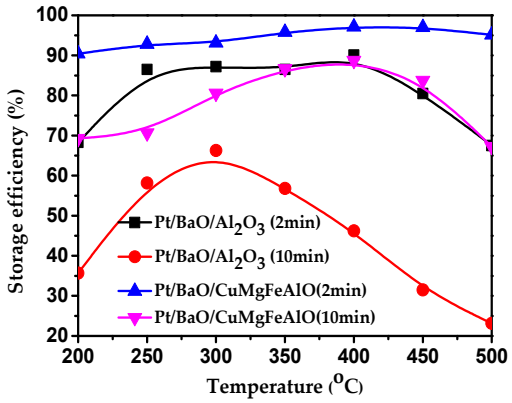

Figure 10. NOx storage efficiency of Pt/BaO/Al_2O_3 and Pt/BaO/CuMgFeAlO catalysts under different temperatures.

2.4.3. NOx-Temperature Programmed Desorption (TPD)

The NOx-TPD profiles of the catalysts are shown in Figure 11. Both catalysts present distinct NOx desorption peak in the range of 200–600 °C. The Pt/BaO/Al_2O_3 catalyst exhibits a single desorption peak at 492 °C, while two major desorption peaks are evident for the Pt/BaO/CuMgFeAlO catalyst at 258 and 481 °C. The low desorption peak (at 258 °C) for the Pt/BaO/CuMgFeAlO catalyst is ascribed to the reduced stability of stored NOx species due to the Cu addition [41]. Moreover, it is obvious that the Pt/BaO/CuMgFeAlO catalyst has a wider NOx desorption range and a higher desorption area than for the Pt/BaO/Al_2O_3 catalyst, implying that the Pt/BaO/CuMgFeAlO catalyst still exhibits an outstanding ability in NOx desorption after coating on the support.

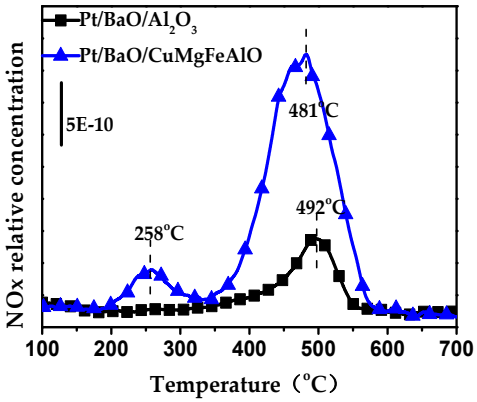

Figure 11. NOx-temperature programmed desorption (TPD) profiles of Pt/BaO/Al_2O_3 and Pt/BaO/CuMgFeAlO catalysts.

2.4.4. NOx Reduction

Figure 12 shows the schematic diagram for the NOx concentrations at the outlets of both catalysts in the periodic lean/rich operation process. The time for the lean and rich burn phases are set at 60 s, respectively. In the lean period, NO is oxidized into NO_2 over precious metal and adsorbed on the catalysts mainly in a form of nitrates. During the rich stage, the NOx stored on the catalysts releases rapidly and then is reduced by the reductants [4], and the time that the NOx concentration for the Pt/BaO/Al_2O_3 catalyst falls to a low level is shorter than for the Pt/BaO/CuMgFeAlO catalyst. The concentrations of N_2O and NH_3 during the rich period were measured by an online mass spectrometry. The selectivities to ammonia (S_{NH_3}) and to nitrogen (S_{N_2}) and the LNT efficiency (ε_{LNT}) were calculated according to the equations introduced in Section 3.3. Table 4 shows the S_{NH_3}, S_{N_2} and ε_{LNT} for the catalysts. In the range of test temperatures, the Pt/BaO/CuMgFeAlO catalyst exhibits lower S_{NH_3}, and higher S_{N_2} and ε_{LNT} than the Pt/BaO/Al_2O_3 catalyst. These results demonstrate that the Pt/BaO/CuMgFeAlO catalyst still retains outstanding performance in NOx reduction after coating on the support.

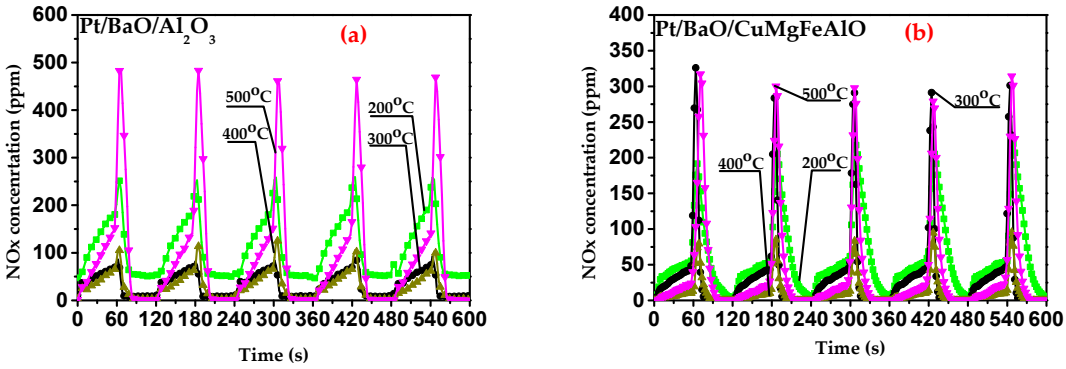

Figure 12. Lean/rich burn operation process of the catalysts under different temperatures. (**a**) Pt/BaO/Al_2O_3; (**b**) Pt/BaO/CuMgFeAlO.

Table 4. S_{NH_3}, S_{N_2} and ε_{LNT} for both catalysts under different temperatures.

Temperature	Pt/BaO/Al_2O_3			Pt/BaO/CuMgFeAlO		
	S_{NH_3} [1]	S_{N_2}	ε_{LNT}	S_{NH_3}	S_{N_2}	ε_{LNT}
200 °C	13.56	86.44	70.66	2.78	97.22	85.64
300 °C	20.80	79.20	74.28	3.00	97.00	90.30
400 °C	9.32	90.68	85.60	0.99	99.01	96.93
500 °C	3.59	96.41	76.69	0.15	99.85	92.80

[1] N_2O is negligible in this work, and thus the S_{NH_3} plus the S_{N_2} is 100 (%).

3. Experimental

3.1. Catalyst Preparation and Coating

The $Cu_{0.6}Mg_{2.4}Fe_{0.5}Al_{0.5}$ hydrotalcite-like compound was prepared by a co-precipitation method [7] where the molar ratio of Cu:Mg:Fe:Al was 0.6:2.4:0.5:0.5. Briefly, the metal nitrates including $Mg(NO_3)_2{\cdot}6H_2O$, $Cu(NO_3)_2{\cdot}3H_2O$, $Fe(NO_3)_3{\cdot}9H_2O$ and $Al(NO_3)_3{\cdot}9H_2O$ (AR, Yuanli, Tianjin, China) were dissolved in de-ionized water to prepare a mixed solution, denoted as solution A. Solution B was also formed containing NaOH and Na_2CO_3 (molar ratio = 1:1) (AR, Yuanli, Tianjin, China). Both solutions were dropwise added into de-ionized water at constant pH (10 ± 0.5) with continuous stirring. The precipitates obtained were placed for 12 h at room temperature, then filtered and washed with de-ionized water. Consequently, the $Cu_{0.6}Mg_{2.4}Fe_{0.5}Al_{0.5}$ hydrotalcite-derived oxide (denoted as CuMgFeAlO) was obtained after drying at 110 °C overnight and calcining at 500 °C in air for 4 h.

In the slurry preparation, the CuMgFeAlO powder was suspended in de-ionized water with continual stirring. Glacial acetic acid (AR, Yuanli, Tianjin, China) was added in the slurry for peptization. At the same time, binder (alumina sol) (AR, Yuanli, Tianjin, China) and additive (polyethylene glycol 1000) (AR, Yuanli, Tianjin, China) were added. The hydrotalcite-based slurry was completely prepared after stirring for 3 h.

Prior to coating, the cordierite support (D × L = 20×40 mm, 400 cells/in^2) was pretreated. Firstly, the support was washed with de-ionized water, then immersed into dilute HNO_3 (AR, Yuanli, Tianjin, China) with a water bath at 80 °C for 30 min. The pretreatment was completed after the cordierite was washed, dried at 120 °C for 12 h and calcined at 500 °C for 4 h.

In the coating process, the pretreated cordierite was immersed into the hydrotalcited-based slurry for 4 min, and then the extra slurry on the support was removed using a ZBM-0.1/8 air pump (OTS, Taizhou, Zhejiang, China). The hydrotalcite-based washcoat-support sample was obtained after drying in a DZF-6020AB oven (Zhongxingweiye Instrument, Beijing, China) at 110 °C for 4 h and calcining in a Lindberg/Blue M muffle furnace (Thermo Scientific, Asheville, NC, USA) at 500 °C for 4 h. In addition, barium acetate (AR, Yuanli, Tianjin, China) and platinum nitrate (AR, Yuanli, Tianjin, China) were added into the above-mentioned slurry with stirring for 3 h, and then the slurry was coated on the cordierite. Eventually, the Pt/BaO/CuMgFeAlO (Pt = 1 wt%, BaO = 20 wt%) monolithic LNT catalyst was prepared after drying and calcination with the same procedures. For comparison, the commercial LNT catalyst with Pt/BaO/Al_2O_3 (Pt = 1 wt%, BaO = 20 wt%) was prepared.

3.2. Characterization of Slurry and Washcoat

Slurry viscosity was measured using an LVDV-III viscometer (Brookfield, Middleboro, MA, USA). Particle size distribution for the slurry was obtained using a LS-POP laser particle size analyzer (OMEC, Zhuhai, Guangdong, China). Low temperature N_2 adsorption-desorption was performed on an NOVA-2000 instrument (Quantachrome, Boynton Beach, FL, USA) to measure the specific surface area. Prior to measurement, the sample (100 mg) was ground into powder in a mortar for 15 min. In order to remove the impurities and moisture, the sample was pretreated at 300 °C in vacuum atmosphere for 3 h, then cooled down to room temperature and started the measurement. X-ray diffraction (XRD) was performed using a Rigaku D/MAC/max 2500 v/pc apparatus with Cu Kα radiation (40 kV, 200 mA, λ = 0.1540560 nm) (Japanese Science, Tokyo, Japan). The scan was operated with a 2θ rate of 2°/min from 5–80°. Scanning electron microscopy (SEM) images of the washcoat and the catalysts were obtained applying an S-4800 scanning electron microscope (Hitachi, Tokyo, Japan).

Washcoat loading (ω) is defined as the extra mass of the support after coating divided by the original mass of the empty cordierite support.

$$\omega\ (\%) = \frac{m_1 - m_0}{m_0} \times 100 \quad (1)$$

where m_1 is the mass of the cordierite support covered with washcoat, m_0 is the mass of the fresh cordierite support without washcoat.

3.3. Characterization of Pt,Ba-Containing Monolithic Catalyst

A ChemBet Pulsar device was applied to carry out temperature programmed desorption (TPD) (Quantachrome, Boynton Beach, FL, USA). Prior to the test, the cordierite-washcoat sample was milled into powder in a mortar for 30 min. Then the powder was pressed into a wafer and sieved into 20–40 meshes. In this experiment, 50 mg of the sample was exposed to pure He at a flow rate of 25 mL/min for 40 min at 400 °C. Then, the same gas was utilized to cool the sample down to 240 °C. At the same time, the gas was shifted to an atmosphere composed by 1500 ppm NO and 10% O_2 (balance, He). The time for NOx adsorption was 90 min. After that, the sample was cooled down to room temperature in pure He. The NOx-TPD measurement was performed by increasing the

temperature to 650 °C at a heating rate of 10 °C/min in pure He. The generation of NOx was measured by a thermal conductivity detector.

The tests of NOx storage and reduction for the catalysts were carried out on a homemade activity evaluation system. A quartz glass tube of the equipment was used as a reaction bed, and the temperature of the reaction bed was controlled by a heating wire. A K-type thermocouple was applied to monitor the reaction temperature, and the gas concentrations entering into the reaction bed were controlled by mass flow meters. The space velocity was set at 20,000 h^{-1}. The gas concentrations at the reactor outlet were measured with an online mass spectrometry (V&F, Absam, Tirol, Austria). Prior to the experiments, the monolithic catalyst was installed into the quartz glass tube, and the catalyst was fully pretreated in a reductive atmosphere where the concentrations of CO, H_2 and C_3H_6 were 500 ppm (balance, N_2), respectively. Then the tests of NOx storage and reduction for the catalysts were performed. In the NOx storage experiment, the catalyst was installed into the quartz glass tube and exposed to a gas mixture containing 10% O_2 and 500 ppm NO (balance, N_2). The time of the adsorption for the catalyst was set at 10 min. The NOx storage test was carried out under different adsorption temperatures. For the NOx reduction test, the atmosphere was periodically altered between lean and rich operation conditions. The gas in the lean period contained 10% O_2 and 500 ppm NO (balance, N_2). In the rich phase, the gas concentrations of CO, H_2 and C_3H_6 were 500 ppm (balance, N_2), respectively. The time of the lean phase and rich phase were set at 60 s, respectively. The NOx reduction test was performed at four temperature conditions.

In the rich conditions, NOx is reduced to N_2, NH_3 and N_2O. Then the activity of the catalyst during lean and rich cycles was calculated by the following equations, as described in [42,43].

The NOx storage efficiency ($\mu_{Storage}$):

$$\mu_{Storage} = \frac{NOx^{stored}}{(NO^{in})_L} \times 100 = \frac{\left(NO^{in}\right)_L - \left(NOx^{out}\right)_L}{(NO^{in})_L} \times 100 \quad (2)$$

where NOx^{stored} is the total amount of NOx stored on the catalyst (mol) in the lean condition, $(NO^{in})_L$ is the NO total amount (mol) entering into the reactor in the lean burn phase, and $(NOx^{out})_L$ is the NOx total amount (mol) measured at the outlet of the reactor.

NOx reduction efficiency (X_R) during the rich phase:

$$X_R = \frac{NOx^{stored} + \left(NO^{in}\right)_R - \left(NOx^{out}\right)_R}{NOx^{stored} + (NO^{in})_R} \times 100 \quad (3)$$

where $(NO^{in})_R$ $(NOx^{out})_R$ is NO (NOx) total amount at the inlet (outlet) of the reactor during the rich period. It is considered that the NOx to be reduced equals to the sum of NOx^{stored} and $(NO^{in})_R$.

The selectivity to NH_3 (N_2O) is defined as the total amount of NH_3 (N_2O) measured at the reactor outlet related to the total amount of reacted NOx.

$$S_{NH_3} = \frac{NH_3{}^{out}}{NOx^{stored} + (NO^{in})_R - (NOx^{out})_R} \times 100 \quad (4)$$

$$S_{N_2O} = \frac{2 \times N_2O^{out}}{NOx^{stored} + (NO^{in})_R - (NOx^{out})_R} \times 100 \quad (5)$$

In a steady NOx storage-reduction cycle, the total amount of the stored NOx and the NO fed in the rich phase equals to the amount of the released NH_3, N_2O, N_2 and a small quantity of NOx without being reduced.

$$NOx^{srored} + \left(NO^{in}\right)_R = NH_3{}^{out} + 2N_2{}^{out} + 2N_2O^{out} + \left(NOx^{out}\right)_R \quad (6)$$

The N_2 generation amount can be deduced by the conservation of nitrogen.

$$2N_2{}^{out} = NOx^{srored} + \left(NO^{in}\right)_R - NH_3{}^{out} - 2N_2O^{out} - \left(NOx^{out}\right)_R \quad (7)$$

$$S_{N_2} = \frac{2 \times N_2{}^{out}}{NOx^{stored} + (NO^{in})_R - (NOx^{out})_R} \times 100 \quad (8)$$

LNT efficiency (ε_{LNT}) is defined as the generation amount of N_2 divided by the total amount of NOx fed during both lean and rich cycles. The LNT efficiency is obtained using the following equation:

$$\varepsilon_{LNT} = \frac{2 \times N_2{}^{out}}{(NO^{in})_L + (NO^{in})_R} \times 100. \quad (9)$$

4. Conclusions

The viscosity of the slurry is strongly affected by pH, solid content, binder and additive. An optimal hydrotalcite-based slurry is obtained after optimization of pH, solid content, binder mass fraction and PEG1000 content to 4, 30 wt%, 4 wt% and 2 wt%, respectively. The optimized slurry presents a similar particle size distribution with the slurry that CuMgFeAlO is included. The cordierite-washcoat sample presents a much higher specific surface area than that of the fresh cordierite support. After coating and calcination, the main phase of the washcoat material is MgO. Cu, Al and Fe uniformly disperse in the CuMgFeAlO material and exist mainly in a form of amorphism. The hydrotalcite-based washcoat is closely contacted with the cordierite substrate, and the Pt/BaO/CuMgFeAlO catalyst still maintains the lamellar texture of the hydrotalcite material. The Pt/BaO/CuMgFeAlO catalyst exhibits better performances in NOx storage and desorption, selectivity to N_2 and LNT efficiency than the Pt/BaO/Al_2O_3 catalyst in the range of tested temperatures, manifesting that the optimized hydrotalcite-based slurry works well after coating on the support.

Author Contributions: This paper was successfully accomplished through cooperation of all authors. Y.Z. (Yue Zhu), B.L. and Y.Z. (Yantao Zhu) designed and performed the experiments and analyzed the data. C.S. and G.L. assisted in manuscript revision. Y.L., W.Z. and Y.W. provided suggestions. Y.Z. (Yue Zhu) wrote the paper.

Funding: This research was funded by the National Natural Science Foundation of China, grant number 51476116, the Tianjin Science and Technology Program, grant number 18PTZWHZ00170 and the Natural Science Foundation of Tianjin, grant number 19JCZDJC40100. The APC was funded by the Tianjin Science and Technology Program.

Conflicts of Interest: The authors declare no conflict of interest.

References

1. Shinjoh, H.; Takahashi, N.; Yokota, K.; Sugiura, M. Effect of periodic operation over Pt catalysts in simulated oxidizing exhaust gas. *Appl. Catal. B* **1998**, *15*, 189–201. [CrossRef]
2. Liu, Z.M.; Woo, S.I. Recent advances in catalytic DeNOx science and technology. *Catal. Rev. Sci. Eng.* **2006**, *48*, 43–89. [CrossRef]
3. Epling, W.S.; Campbell, L.E.; Yezerets, A.; Currier, N.W.; Parks, J.E. Overview of the Fundamental reactions and degradation Mechanisms of NOx storage/reduction catalysts. *Catal. Rev. Sci. Eng.* **2004**, *46*, 163–265. [CrossRef]
4. Matsumoto, S. Recent advances in automobile exhaust catalysts. *Catal. Today* **2004**, *90*, 183–190. [CrossRef]
5. Roy, S.; Baiker, A. NOx storage-reduction catalysis: From mechanism and materials properties to storage-reduction performance. *Chem. Rev.* **2009**, *109*, 4054–4091. [CrossRef]
6. Fornasaria, G.; Glfcklerb, R.; Livia, M.; Vaccari, A. Role of the Mg/Al atomic ratio in hydrotalcite-based catalysts for NOx storage/reduction. *Appl. Clay Sci.* **2005**, *29*, 258–266. [CrossRef]
7. Centi, G.; Fornasari, G.; Gobbi, C.; Livi, M.; Trifiro, F.; Vaccari, A. NOx storage-reduction catalysts based on hydrotalcite. Effect of Cu in promoting resistance to deactivation. *Catal. Today* **2002**, *73*, 287–296. [CrossRef]
8. Braterman, P.S.; Xu, Z.P.; Yarberry, F. *Handbook of Layered Materials*; Auerbach, S.M., Carrado, K.A., Dutta, P.K., Eds.; Marcel Dekker Inc.: New York, NY, USA, 2004; p. 373.

9. Liu, L.; Li, S.L.; An, Y.L.; Sun, X.C.; Wu, H.L.; Li, J.Z.; Chen, X.; Li, H.D. Hybridization of Nanodiamond and CuFe-LDH as Heterogeneous Photoactivator for Visible-Light Driven Photo-Fenton Reaction: Photocatalytic Activity and Mechanism. *Catalysts* **2019**, *9*, 118. [CrossRef]
10. Cavani, F.; Trifirò, F.; Vaccari, A. Hydrotalcite-type anionic clays: Preparation, properties and applications. *Catal. Today* **1991**, *11*, 173–301. [CrossRef]
11. Li, B.S.; Yuan, S.L. Synthesis, characterization, and evaluation of TiMgAlCu mixed oxides as novel SOx removal catalysts. *Ceram. Int.* **2014**, *40*, 11559–11566. [CrossRef]
12. Wang, Z.P.; Li, Q.; Wang, L.G.; Shangguan, W.F. Simultaneous catalytic removal of NOx and soot particulates over CuMgAl hydrotalcites derived mixed metal oxides. *Appl. Clay Sci.* **2012**, *55*, 125–130. [CrossRef]
13. Li, Q.; Meng, M.; Tsubaki, N.; Li, X.G.; Li, Z.Q.; Xie, Y.N.; Hu, T.D.; Zhang, J. Performance of K-promoted hydrotalcite-derived CoMgAlO catalysts used for soot combustion, NOx storage and simultaneous soot-NOx removal. *Appl. Catal. B Environ.* **2009**, *91*, 406–415. [CrossRef]
14. Li, Q.; Meng, M.; Dai, F.F.; Zha, Y.Q.; Xie, Y.N.; Hu, T.D.; Zhang, J. Multifunctional hydrotalcite-derived K/MnMgAlO catalysts used for soot combustion, NOx storage and simultaneous soot–NOx removal. *Chem. Eng. J.* **2012**, *184*, 106–112. [CrossRef]
15. Sikander, U.; Sufian, S.; Salam, M.A. Synthesis and Structural Analysis of Double Layered Ni-Mg-Al Hydrotalcite Like Catalyst. *Procedia Eng.* **2016**, *148*, 261–267. [CrossRef]
16. Martin, H.; Jaroslav, K.; Karel, F.; Aleš, V. Mg-Fe mixed oxides and their rehydrated mixed oxides as catalysts for transesterification. *J. Clean. Prod.* **2017**, *161*, 1423–1431.
17. Tahir, N.; Abdelssadek, Z.; Halliche, D.; Saadi, A.; Cherifi, O.; Bachari, K. Study of the benzylation of aromatics over Mg-Cr-hydrotalcite catalysts. *Stud. Surf. Sci. Catal.* **2008**, *174*, 1287–1290.
18. Jabłonska, M.; Palomares, A.E.; Chmielarz, L. NOx storage/reduction catalysts based on Mg/Zn/Al/Fe hydrotalcite-like materials. *Chem. Eng. J.* **2013**, *231*, 273–280. [CrossRef]
19. Wang, R.N.; Wu, X.; Zou, C.L.; Li, X.J.; Du, Y.L. NOx Removal by Selective Catalytic Reduction with Ammonia over a Hydrotalcite-Derived NiFe Mixed Oxide. *Catalysts* **2018**, *8*, 384. [CrossRef]
20. Dai, F.F.; Zhang, Y.X.; Meng, M.; Zhang, J.; Zheng, L.R.; Hu, T.D. Enhanced soot combustion over partially substituted hydrotalcite-drived mixed oxide catalysts CoMgAlLaO. *J. Mol. Catal. A Chem.* **2014**, *393*, 68–74. [CrossRef]
21. Tomasic, V.; Jovic, F. State-of-the-art in the monolithic catalysts/reactors. *Appl. Catal. A* **2006**, *311*, 112–121. [CrossRef]
22. Nijhuis, T.A.; Beers, A.E.W.; Vergunst, T.; Hoek, I.; Kapteijn, F.; Moulijn, J.A. Preparation of monolithic catalysts. *Catal. Rev. Sci. Eng.* **2001**, *43*, 345–380. [CrossRef]
23. Blachou, V.; Goula, D.; Philippopoulos, C. Wet milling of alumina and preparation of slurries for monolithic structures impregnation. *Ind. Eng. Chem. Res.* **1992**, *31*, 364–369. [CrossRef]
24. Shimrock, T.; Taylor, R.D.; Collins, J. Method of impregnating ceramic monolithic structures with predetermined amounts of catalyst. Europe Patent 0157651, 9 October 1985.
25. Gao, J.L.; Liu, J.X.; Zhang, D.Q.; Li, D.F.; Zhang, J.R. Influence of Additive on Al_2O_3 washcoat of Porous Ceramic Substrate. *J. Chem. Eng. Chin. Univ.* **2006**, *20*, 142–146.
26. Li, B. Study on the NOx Reduction for Diesel Engines Using the Modified-Hydrotalcite Derived LNT catalyst. Ph.D. Thesis, Tianjin University, Tianjin, China, 2018.
27. Agrafiotis, C.; Tsetsekou, A. Deposition of meso-porous g-alumina coatings on ceramic honeycombs by sol-gel methods. *J. Eur. Ceram. Soc.* **2002**, *22*, 423–434. [CrossRef]
28. Jiang, P.P.; Lu, G.Z.; Guo, Y.; Guo, Y.L.; Zhang, S.H.; Wang, X.Y. Preparation and properties of a γ-Al_2O_3 washcoat deposited on a ceramic honeycomb. *Surf. Coat. Technol.* **2005**, *190*, 314–320. [CrossRef]
29. Pereda-Ayo, B.; López-Fonseca, R.; González-Velasco, J.R. Influence of the preparation procedure of NSR monolithic catalysts on the Pt-Ba dispersion and distribution. *Appl. Catal. A Gen.* **2009**, *363*, 73–80. [CrossRef]
30. Pereda-Ayo, B.; González-Velasco, J.R. NOx Storage and Reduction for Diesel Engine Exhaust Aftertreatment. In *Diesel Engine—Combustion, Emissions and Condition Monitoring*, 1st ed.; Bari, S., Ed.; Intech: Rijeka, Croatia, 2013; pp. 161–196.
31. Agrafiotis, C.; Tsetsekou, A. The effect of processing parameters on the properties of γ-alumina washcoats deposited on ceramic honeycombs. *J. Mater. Sci.* **2000**, *35*, 951–960. [CrossRef]
32. Adamowska, M.; Costa, P.D. Structured Pd/γ-Al_2O_3 Prepared by Washcoated Deposition on a Ceramic Honeycomb for Compressed Natural Gas Applications. *J. Nanopart.* **2015**, *9*. [CrossRef]

33. Tian, J.Y.; Lu, J.S.; Wu, H. Effect of Additive Polyethylene Glycol on γ-Al_2O_3 Washcoat Properties of Cordierite Ceramic Honeycomb. *J. Chem. Eng. Chin. Univ.* **2010**, *24*, 167–170.
34. Zheng, J.; Tian, X.; Yu, K.; Wang, L.; Yang, C.; He, M. Hydrothermal Synthesis and Characterization of Regular and Homogeneous Nanocrystalline Hydrotalcite. *Acta Chim. Sin.* **2006**, *64*, 2231–2234.
35. Tascón, A. Influence of particle size distribution skewness on dust explosibility. *Powder Technol.* **2018**, *338*, 438–445. [CrossRef]
36. Yi, H.H.; Xie, X.Z.; Tang, X.L.; Zhao, S.Z.; Yang, K.; Huang, Y.H.; Yang, Z.Y. Demonstration of low-temperature toluene degradation mechanism on hydrotalcite-derived oxides with ultrasonic intervention. *Chem. Eng. J.* **2019**, *374*, 370–380. [CrossRef]
37. Jabłońska, M.; Nothdurft, K.; Nocuń, M.; Girmanc, V.; Palkovits, R. Redox-performance correlations in Ag–Cu–Mg–Al, Ce–Cu–Mg–Al, and Ga–Cu–Mg–Al hydrotalcite derived mixed metal oxides. *Appl. Catal. B Environ.* **2017**, *207*, 385–396. [CrossRef]
38. Luo, J.Y.; Meng, M.; Li, X.; Li, X.G.; Zha, Y.Q.; Hu, T.D.; Xie, Y.N.; Zhang, J. Mesoporous Co_3O_4-CeO_2 and Pd/Co_3O_4-CeO_2 catalysts: Synthesis characterization and mechanistic study of their catalytic properties for low-temperature CO oxidation. *J. Catal.* **2008**, *254*, 310–324. [CrossRef]
39. Vijay, R.; Sakurai, H.; Snively, C.M.; Lauterbach, J. Mechanistic Investigation of Co Containing NOx Traps. *Top. Catal.* **2009**, *52*, 1388–1399. [CrossRef]
40. Basile, F.; Fornasari, G.; Livi, M.; Tinti, F.; Trifirò, F.; Vaccari, A. Performance of new Pt and Pt-Cu on hydrotalcite-derived materials for NOx storage/reduction. *Top. Catal.* **2004**, *30*, 223–227. [CrossRef]
41. Muñoz, V.; Zotin, F.M.Z.; Palacio, L.A. Copper-aluminum hydrotalcite type precursors for NOx abatement. *Catal. Today* **2015**, *250*, 173–179. [CrossRef]
42. Pereda-Ayo, B.; Duraiswami, D.; Delgado, J.J.; López-Fonseca, R.; Calvino, J.J.; Bernal, S.; González-Velasco, J.R. Tuning operational conditions for efficient NOx storage and reduction over a Pt-Ba/Al_2O_3 monolith catalyst. *Appl. Catal. B Environ.* **2010**, *96*, 329–337. [CrossRef]
43. Pereda-Ayo, B.; Duraiswami, D.; González-Marcos, J.A.; González-Velasco, J.R. Performance of NOx storage-reduction catalyst in the temperature-reductant concentration domain by response surface methodology. *Chem. Eng. J.* **2011**, *169*, 58–67. [CrossRef]